Some Considerations in The Evaluation of Seasat-A Scatterometer (SASS) Measurements

ISIDORE HALBERSTAM

Jet Propulsion Laboratory, California Institute of Technology, Pasadena, CA 91103

(Manuscript received 4 December 1978, in final form 30 November 1979)

ABSTRACT

A study is made of the geophysical algorithms relating the Seasat-A scatterometer (SASS) backscatter measurements σ° with a wind parameter. It is shown that although σ° is closely related to surface features, identification with surface layer parameters such as friction velocity u^* or the roughness length z_0 is difficult from both theoretical and practical considerations. It is shown how surface truth in the form of wind speeds and coincident stability can be used to derive either u^* or the equivalent neutral wind u_N at an arbitrary height. It is also shown that derived u^* values are sensitive to contested formulations relating u^* to z_0, while derived u_N values are not. Also, derived quantities are seen to be more sensitive to changes in positive stability than to change in unstable conditions. Examples of geophysical verification is demonstrated using values obtained from the Gulf of Alaska Seasat Experiment (GOASEX). Results of this verification show very little sensitivity to the type of wind parameter employed. It is suggested that this insensitivity is due mainly to large scatter in the SASS and surface truth data.

1. Introduction

Aboard Seasat-A, launched in June 1978, was the Seasat-A scatterometer (SASS), designed to measure Bragg scattering from the ocean surface. The backscatter σ° has been theoretically linked to a wind parameter long before the launch of Seasat (Moore and Pierson, 1971; Bradley, 1971). Since the premature termination of Seasat's transmission in October 1978, an intense verification effort has been taking place for all of Seasat's instruments. A major surface truth comparison activity stems from the Gulf of Alaska Seasat Experiment (GOASEX). Intense workshops were held in January and June 1979, where Seasat output was examined in the light of many ship, buoy and aircraft reports. A summary of this activity was made by Born *et al.* (1979a,b), Jones *et al.* (1979), Tapley *et al.* (1979), Gonzalez *et al.* (1979) and Lipes *et al.* (1979). With regard to SASS verification, an ambiguity has always existed concerning the geophysical parameter best suited to serve as the algorithm product. Many researchers refer to the wind speed as the verification product (Bradley, 1971; Young and Moore, 1977; Moore *et al.*, 1979; Ross and Jones, 1978). Others, however, have consistently assumed that wind stress or friction velocity u^* would make a better verification product (Pierson and Stacy, 1973; Jones *et al.*, 1978b, Jones and Schroeder, 1978). Pierson (1978) felt that neutral winds at an arbitrary 19.5 m above the surface are primary verification parameters, because of problems arising in obtaining accurate u^* data, measured or derived. To understand the ambiguity surrounding the verification of SASS, this paper intends to investigate the nature of SASS, demonstrate its relationship with the surface layer, and apply some of these principles to a comparison of SASS data with GOASEX surface truth.

2. The scatterometer

SASS was designed to beam a radar pulse at the sea surface and to measure the backscatter produced by the surface configuration. The designed frequency, approximately 13.9 GHz, is sensitive to the capillary wave structure at the sea surface. The mechanics of capillary wave generation is not completely understood, but as Phillips (1977) explains, it should be related to the turbulent structure of the surface layer. If so, the backscatter σ° should be a function of some surface layer variable. Of course, other factors may influence the observed σ° such as slicks, ocean spray and fetch. These effects have been discussed by Hühnerfuss *et al.* (1978) and Ross and Jones (1978) among others. The latter concluded that fetch has only a secondary effect on the backscatter. Precipitation has an attenuating effect on the radar and its effect must be correctly modeled before areas of precipitation can be correctly analyzed (Jones *et al.*, 1979). Barring these interferences, σ° should be relatable to three primary variables: the beam incidence angle θ, the polarity, and a vector parameter in the planetary boundary layer. This relationship has often been given (Young

0022-3670/80/040623-10$06.50

and Moore, 1977; Jones and Schroeder, 1978; among others) as

$$\sigma^\circ = A(\theta,\chi) + B(\theta,\chi)\log y, \tag{1}$$

where χ is the crosswind direction (i.e., the difference between the satellite azimuth and the wind direction) and y is either friction velocity or wind speed depending on the authority quoted. A and B are harmonic functions of χ with the amplitudes dependent on θ. Derivations of the coefficients and their dependency on their parameters are based on observations made with the scatterometer in areas of surface truth. This process is a major ingredient in the various algorithms produced for SASS. Thus algorithms produced by Jones *et al.* (1978b), Pierson and Salfi (1978) or Moore *et al.* (1979) all require a body of surface truth that can be used in conjunction with airborne or spaceborne scatterometer data. Prior to the launch of Seasat, experiments were in the form of aircraft overflights during JONSWAP (Jones *et al.*, 1978a) or during the Skylab mission (Cardone *et al.*, 1976). These have provided tables for the calculation of the coefficients in the function $\sigma^\circ(\theta,y,\chi)$. The surface truth available in these experiments was only in the form of wind speeds at various heights. Boundary-layer models were required to compute winds at a fixed height or to derive values for u^*.

Once σ° is known as a function of its three significant variables, it is theoretically possible to invert the relationship and obtain values for y and χ, if two equations in σ° are provided. Thus, SASS was designed to produce two values of σ° at a given point, from two orthogonal beams so that $\chi_2 = \chi_1 + 90°$. The system of equations

$$\left.\begin{aligned}\sigma_1^\circ &= f(\theta,y,\chi)\\ \sigma_2^\circ &= f(\theta, y, \chi + 90°)\end{aligned}\right\}, \tag{2}$$

is now solvable for y and χ giving wind speed (or stress) and its direction. Since the functions are harmonic in χ, however, they will furnish four possible solutions for y and χ. The true physical solution will have to be determined empirically, e.g., by alignment with the gradient wind. By eliminating this ambiguity, one can then arrive at a unique estimate for y and χ.

3. The surface layer

To understand the uncertainty involving the variable y, one must first delve into the relationship between σ° and the atmospheric surface layer. As mentioned earlier, σ° is a measure of the backscatter, mainly from capillary waves, which in turn are related to the turbulent structure of the atmosphere near the surface. Turbulent fluxes of heat and momentum are considered constant in a region near the surface known as the constant-flux layer or, simply, the surface layer.

In this region, the wind and temperature profiles are logarithmic with adjustments for stability. By similarity theory, the adjustment terms must be functions of the nondimensional variable z/L, where L is the characteristic Monin-Obhukov length-dependent on the ratio of momentum flux to heat flux. The profile equations can thus be expressed as

$$\left.\begin{aligned}u &= u^*[(\ln(z/z_0) + \psi_m(z/L)]/k\\ \theta_v &= \theta_{vs} + \theta_v^*[(\ln(z/z_0) + \psi_h(z/L)]/k\end{aligned}\right\}, \tag{3}$$

where the symbols with asterisks are characteristic surface flux parameters: u is the wind speed at a specific height z and θ_v the virtual potential temperature at the same height. The similar behavior of humidity and sensible heat flux as reported by Dyer (1967) allows combining the two expressions into a single one involving virtual temperatures. θ_{vs} is the surface virtual temperature, k the Von Kármán constant (0.35), and ψ_m and ψ_h are the similarity functions for momentum and heat. The roughness parameter z_0 is taken as a variable over the oceans dependent solely on the wind stress coefficient u^*, as will be discussed later.

The Monin-Obhukov length L can be given in terms of the surface parameters as

$$L = \bar{\theta}_v u^{*2}(gk\theta_v^*)^{-1}, \tag{4}$$

where $\bar{\theta}_v$ is a mean virtual temperature in the surface layer. Eqs. (3) and (4) form a closed set of equations which may be solved either for the fluxes given the profiles or for the profiles given the fluxes. This all depends, however, on finding a suitable expression for z_0.

Over land, z_0 is ordinarily assumed constant depending on the surface features. Lo (1977) has recently taken exception to this and maintains that z_0 should be dependent on wind speed and direction. Over the oceans the effect of wind is even more pronounced, due mainly to the wind's action in changing the surface.

Early studies by Charnock (1955) uniquely related the roughness parameter to the wind stress; these were followed by further refinements by Cardone (1969), Garratt (1977) and Pierson (1978) who still assumed z_0 was a unique function of u^*. Kitaigorodskii and Zaslavskii (1974), on the other hand, believed that some correction would be necessary for swell and wind fetch. Garratt (1977) discusses their thesis but concludes that the body of assembled data supports a simple z_0–u^* relationship. For purposes of this study, then, we will assume that z_0 can be uniquely defined in terms of u^* by one of the three relationships mentioned above (referred to as C, G and P for Cardone, Garratt and Pierson, respec-

tively). These relationships are as follows:

$$\left.\begin{aligned} \text{C:}\quad & z_0 = 0.684/u^* + 4.28 \times 10^{-5}\, u^{*2} \\ & \qquad - 0.0443 \\ \text{G:}\quad & z_0 = 1.469 \times 10^{-5}\, u^{*2} \\ \text{P:}\quad & z_0 = 0.3905/u^* + 1.604 \times 10^{-5}\, u^{*2} \\ & \qquad - 0.017465 \end{aligned}\right\}, \quad (5)$$

where u^* is expressed in centimeters per second and z_0 is given in centimeters. Fig. 1 shows z_0 as a function of u^* for the three formulas. The three curves converge at about $u^* = 20$ cm s^{-1} below which C and P show an increase in z_0, while G continues to show a decline. Note, also, that P was designed to approximate C for low values of u^* and G for high values. Employing the Businger *et al.* (1971) relationship for the similarity functions, Eqs. (1), (3) and (4) form a closed set, yielding any three of the variables u^*, θ_v^*, $\Delta\theta_v$, u or z, when the remaining terms are known.

4. Verification in the surface layer

In order to verify the potential of SASS to furnish values of u^*, one must be careful of various factors in analyzing surface truth. Among these are 1) the magnitude and persistence of the wind speed, 2) the stability of the atmosphere, 3) the height of the anemometer and 4) the particular model invoked to derive u^*.

The turbulent fluctuations of a wind record could negate the value of an observation if sufficient averaging times are not employed. This problem has been addressed by Pierson *et al.* (1979) who found that averaging times of 3 h are needed for wind data to be compatible with the SASS footprint. No known source of wind speed uses more than 30 min and even these are rare. The truncated averaging time will add more than a 1 m s^{-1} error to the available surface truth.

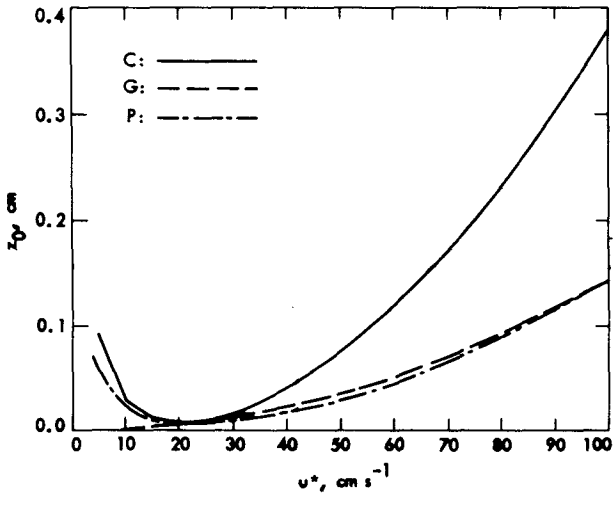

FIG. 1. z_0 as a function of u^* for the C (solid line), G (broken line) and P (dot-dash) formulas.

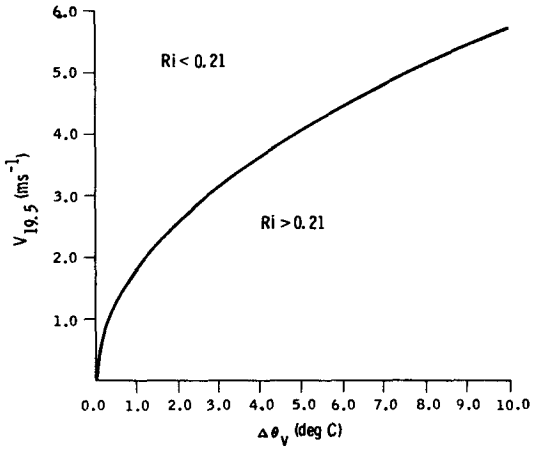

FIG. 2. Parabolic section depicting $\mathrm{Ri_B} = gz\Delta\theta_v(\bar{\theta}_v u^2)^{-1} = 0.21$, with $\bar{\theta}_v = 280.0$ K. The curve separates the turbulent region from the laminar region ($\mathrm{Ri_B} > 0.21$).

The magnitude of the wind speed is important for several reasons. First, it must exceed some critical value before capillary waves are generated. σ° will not be sensitive to wind speeds below that value. (The critical value has been estimated at between 2 and 4 m s^{-1}.) Second, the capillary wave spectrum will saturate at some upper limit of the wind speed. Beyond that speed, σ° will not vary significantly. Because of sparse surface truth beyond 25 m s^{-1}, the upper limit has not been determined. Third, in conjunction with stability and observation height, wind speed will determine whether (3)–(5) can be used in determining u^*. For unstable and neutral atmospheres, there will always be a u^* for any given u. For stable atmospheres there is a cutoff value dependent on the bulk Richardson number $\mathrm{RI_B}$ so that if $\mathrm{Ri_B} \geqslant 0.21$, no solution for u^* can be found. Fig. 2 shows the parabolic section dividing the turbulent from nonturbulent regimes as a function of wind speed at 19.5 m and $\Delta\theta_v$ (air-sea virtual temperature difference) with an assumed $\bar{\theta}_v$ of 280.0 K. For low wind speeds, low stability values will still lie outside the turbulent range. But for values of $u > 5$ m s^{-1}, many stability values commonly found in the ocean render $\mathrm{Ri} < 0.21$.

Stability in conjunction with wind speeds is a necessary ingredient in furnishing surface truth parameters such as u^* or the equivalent neutral wind u_N. Yet not all stability information obtained from conventional sources is reliable. NOAA buoys and weatherships offer high-caliber surface truth, but buoys do not measure humidity, which may become important over the ocean. Commercial ships deliver poorer quality information; sea surface tem-

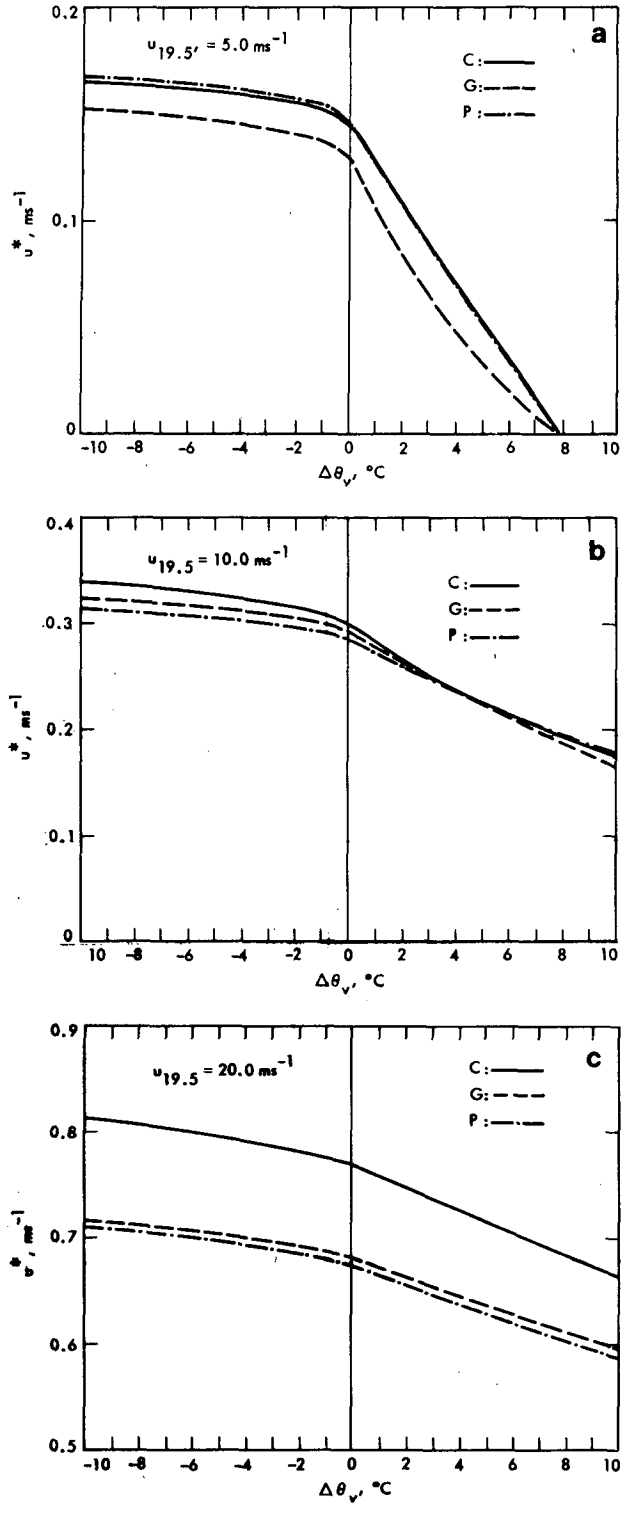

FIG. 3. u^* as a function of stability ($\Delta\theta_v$) for each of C, G and P formulas given wind speeds at 19.5 m of (a) 5, (b) 10 and (c) 20 m s^{-1}.

peratures can be off by ±2°C and wind speeds are averaged for only brief periods. It would be informative to study the effect of stability on estimating u^* or u_N according to each of C, G and P in (5).

Determining u^* from (3)–(5) given $\Delta\theta_v$ and u at a specific height z, requires a double iteration for unstable cases and one iteration for stable. Details of the iterations in the unstable case can be found in the Appendix. Figs. 3a–3c show the dependency of u^* on stability for observed winds at 19.5 m of 5.0, 10.0 and 20.0 m s^{-1}, respectively. The three curves on each chart represent the C, G and P relationships of (5). Immediately noticeable is the strong dependency of u^* on stability especially for light winds. The percentage difference between the models is appreciable with only a slight decline toward positive stability. For increased winds the difference between models increases. This means that errors in comparisons with u^* will result from uncertainties in modeling and poor stability information. Assuming neutrality will involve minor errors for unstable conditions ($\lesssim$6%) but substantially larger errors for stable conditions. Differences between models can account for ~15% of the value of u^*.

By calibrating SASS against a different parameter, u_N for instance, the model ambiguity may be resolved. Pierson (1978) recommended comparisons with neutral winds at 19.5 m (mean ship anemometer height). His illustrations, however, do not focus on non-neutral cases. Instead, he demonstrated that winds observed at any level in a neutral atmosphere can be normalized to 19.5 m using any u^*–z_0 model without incurring significant error. The same result holds true regardless of stability. Figs. 4a–4c show the values of the derived 19.5 m neutral wind given values of u at 50 m of 5, 10 and 20 m s^{-1}, respectively. Ignoring stability would again be acceptable, except in stable atmospheres, but differences due to model choice are negligible. This can be understood if we equate the observed wind speed at a given height z with itself using two different models of $u^*(z_0)$:

$$\frac{u_1^*}{k}\left[\ln\frac{z}{z_{0_1}} + \psi\left(\frac{z}{L_1}\right)\right] = \frac{u_2^*}{k}\left[\ln\frac{z}{z_{0_2}} + \psi\left(\frac{z}{L_2}\right)\right], \quad (6)$$

where the subscripts indicate the different models. The difference between effective neutral winds at the same height would then be given by

$$\frac{u_1^*}{k}\ln\frac{z}{z_{0_1}} - \frac{u_2^*}{k}\ln\frac{z}{z_{0_2}} = \frac{u_1^*}{k}\psi\left(\frac{z}{L_1}\right) - \frac{u_2^*}{k}\psi\left(\frac{z}{L_2}\right). \quad (7)$$

The ratio of z to L, especially in near-neutral conditions, is nearly the same for all $u^*(z_0)$ models. The difference between the neutral winds is essentially proportional to the differences between u_1^* and u_2^* with a multiplier less than 1 in near-neutral conditions. This leads to insignificant magnitudes in the

differences between neutral wind speeds. The same reasoning applies to normalizing observations made at heights different from the standard height, where only a small addition would be made to the right-hand side of (7). Indeed, the effect of "moving" observations of 15 m s^{-1} from any height $\leq$ 150 m to 19.5 m can be seen in Figs. 5a and 5b for air-sea temperature differences of 0.0 and +3.0°C, respectively. Again, it is obvious that adjustment for observation heights is fairly independent of a u^*-z_0 model.

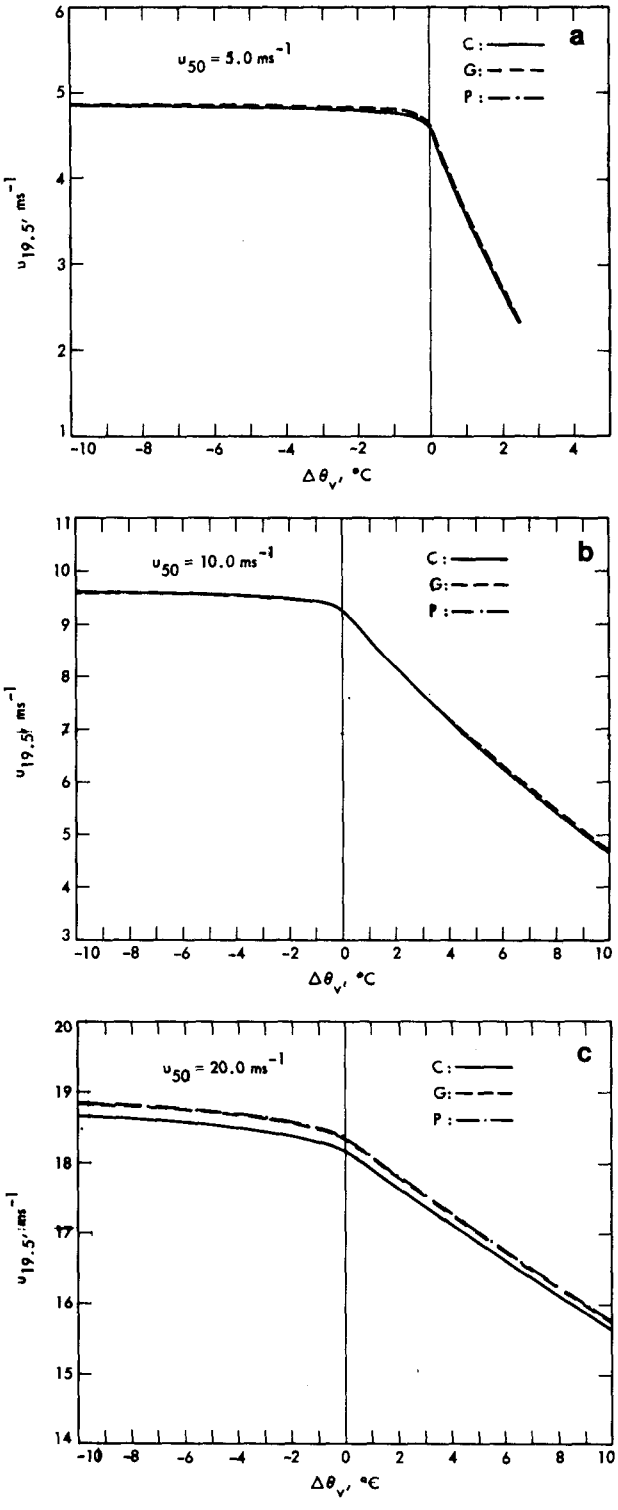

FIG. 4. Wind speeds at 19.5 m as a function of stability ($\Delta\theta_v$), given wind speeds at 50 m of (a) 5, (b) 10 and (c) 20 m s^{-1}. P is coincident with C for (a) and (b).

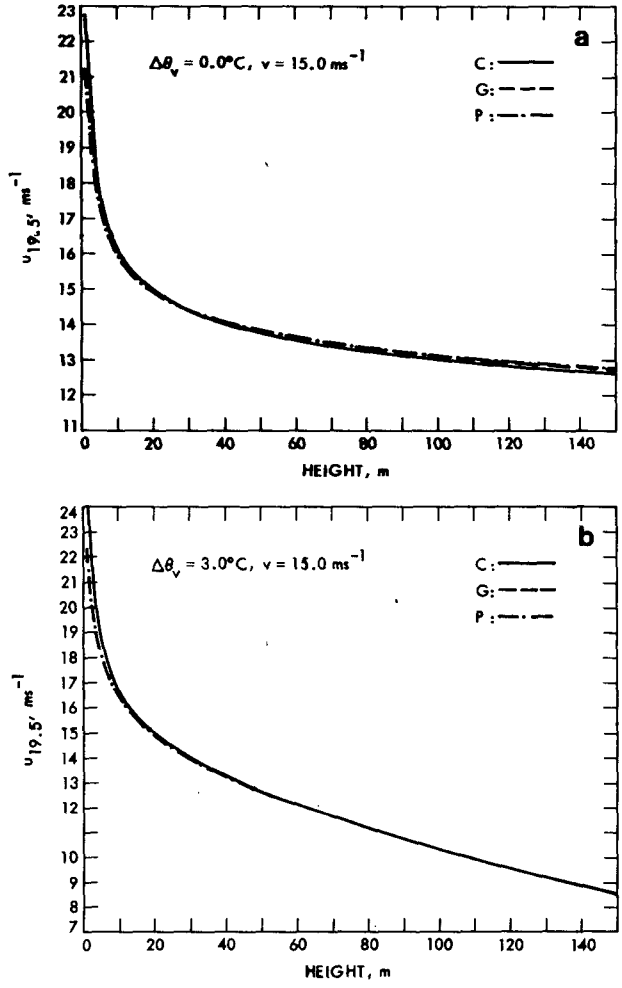

FIG. 5. Wind speeds at 19.5 m as a function of the height of an observed 15 m s^{-1} wind for (a) $\Delta\theta_v$ = 0.0 and (b) $\Delta\theta_v$ = 3.0°C. P is coincident with G in (b).

5. Comparison with GOASEX Data

Most of the problems discussed in the preceding sections were confronted during the GOASEX workshops. These workshops were assembled in order to verify SASS data against a body of surface truth. Surface measurements were mainly in the form of buoy data from the nine NOAA buoys located in the Gulf of Alaska. Other sources of information were the Canadian Weathership P and the NOAA research vessel *Oceanographer*. Ships of opportunity were used in some workshop studies but they will be ignored here because of the generally poor quality of data they provide.

TABLE 1. Regression statistics calculated for σ° versus various wind variables for each polarization and selected incidence angle, θ_i. r is the correlation coefficient, m the slope of the regression line, b the y intercept and σ_u refers to the standard deviation of the variable. Size refers to the sample size for each case.

Variable	Polarization	θ_i	r	m	b	σ_u	Size
u	H	25	0.893	0.750	−2.39	0.577	29
	H	35	0.873	0.901	−3.60	0.614	26
	H	45	0.968	1.076	−4.63	0.545	16
	H	55	0.880	1.021	−4.94	0.521	8
	V	25	0.922	0.649	−2.01	0.568	30
	V	35	0.931	0.867	−3.12	0.599	28
	V	45	0.945	1.171	−4.35	0.536	18
	V	55	0.984	0.794	−3.58	0.521	8
u_N	H	25	0.876	0.786	−2.52	0.555	29
	H	35	0.861	0.959	−3.77	0.569	26
	H	45	0.965	1.094	−4.69	0.534	16
	H	55	0.818	0.891	−4.64	0.555	8
	V	25	0.909	0.684	−2.12	0.532	30
	V	35	0.922	0.924	−3.29	0.558	28
	V	45	0.965	1.22	−4.48	0.525	18
	V	55	0.981	0.743	−3.46	0.555	8
u^* [C]	H	25	0.844	0.735	0.150	0.557	29
	H	35	0.838	0.924	−0.480	0.575	26
	H	45	0.955	0.985	−1.05	0.587	16
	H	55	0.868	0.840	−1.63	0.621	8
	V	25	0.883	0.643	0.205	0.550	30
	V	35	0.908	0.893	−0.113	0.568	28
	V	45	0.944	1.08	−0.439	0.582	18
	V	55	0.975	0.660	−1.01	0.621	8
u^* [G]	H	25	0.878	0.652	0.091	0.652	29
	H	35	0.861	0.793	−0.591	0.688	26
	H	45	0.966	0.911	−1.06	0.642	16
	H	55	0.820	0.745	−1.68	0.666	8
	V	25	0.911	0.567	0.147	0.643	30
	V	35	0.923	0.765	−0.224	0.674	28
	V	45	0.965	1.02	−0.427	0.631	18
	V	55	0.981	0.619	−0.995	0.666	8
u^* [P]	H	25	0.861	0.794	0.267	0.525	29
	H	35	0.850	0.984	−0.352	0.547	26
	H	45	0.962	1.072	−0.880	0.543	16
	H	55	0.850	0.896	−1.52	0.574	8
	V	25	0.898	0.694	0.305	0.518	30
	V	35	0.917	0.951	0.010	0.538	28
	V	45	0.953	1.180	−0.249	0.537	18
	V	55	0.980	0.717	−0.894	0.574	8

Various comparisons of derived winds with observed winds converted to neutral winds at 19.5 m were made and their results reported by Born *et al.* (1979b) and Jones *et al.* (1979). In this study, the observed values of σ° were compared with several wind variables to determine which of them is best predicted by SASS. Most of the buoys had anemometers at heights of 10 m. Air temperatures were provided at the same height but no humidity parameter was provided. Sea surface temperature was also measured, from which the assumed saturated specific humidity could be derived. Eqs. (3)–(5) were employed to derive u_N and three values of u^* for C, G and P, respectively. Because of the lack of humidity readings, θ was used instead of θ_v in computing the fluxes. This may have a significant effect, especially where the air was dry. P was used in deriving u_N but, as discussed earlier, little difference results when using any of the other models.

The σ°'s that were within 75 km of the observation point were used for comparisons with the wind variables at that point. First, they had to be normalized to an arbitrary wind direction and specific incidence angles. The σ°'s were brought to values representing the downwind direction and incidence angles θ_i = 25, 35, 45, and 55° (SASS observations at $\theta < 20°$ were not included in the comparison) by calculating

$$\Delta\sigma^\circ = \sigma^\circ(\theta_0, \chi_0, u_0) - \sigma^\circ(\theta_i, \chi_D, u_0) \qquad (8)$$

and subtracting it from the observed σ°. Here the σ° represents the theoretical values derived from the Wentz algorithm; θ_0, χ_0 and u_0 are the observed incidence angle, crosswind angle and wind speed; θ_i are the selected incidence angles; and χ_D is the downwind angle (180°). The normalized σ°'s are then grouped by incidence angle and weight-averaged by distance to the spot observation. This results in matched σ° and wind variables for each incidence angle. Regression statistics were obtained for σ° versus u, u_N and three values of u^* from (5). Results from this analysis appear in Table 1.

The correlation coefficients do not change drastically regardless of which variable is chosen for comparison. Yet, the scatter for u is generally greater than for u_N, as can be seen from the standard deviation σ_u. The intercepts and slopes are also different mainly because most observations are from buoys with 10 m anemometers, while u_N is calculated at 19.5 m resulting in $u_N > u$. Figs. 6a and 6b show the points and regression lines for σ° versus u and u_N, respectively. For low values of σ°, the scatter increases, while for higher incidence angles the slope increases until ~55° when there is a sudden reversal. The strange behavior at 55° is due mainly to the small sample size and because the scatterometer reaches the limits of its capability at ~60°.V polarization seems to give slightly better correlations than H polarization—an expected result.

The disturbing result that adjustments for stability and height do not affect the correlations significantly indicates that considerable scatter exists in the σ° data from SASS. This was determined by computing the model-derived σ°, given the satellite's incidence angle, the observed wind direction and the known azimuth angle at the surface observation points. The σ°'s were then separated into incidence angle groups. Unlike the previous comparison, the values of σ° were not altered or moved, simply grouped by θ. Thus, the label 25° indicates information for all σ° that were observed at $20° < \theta \leq 30°$,

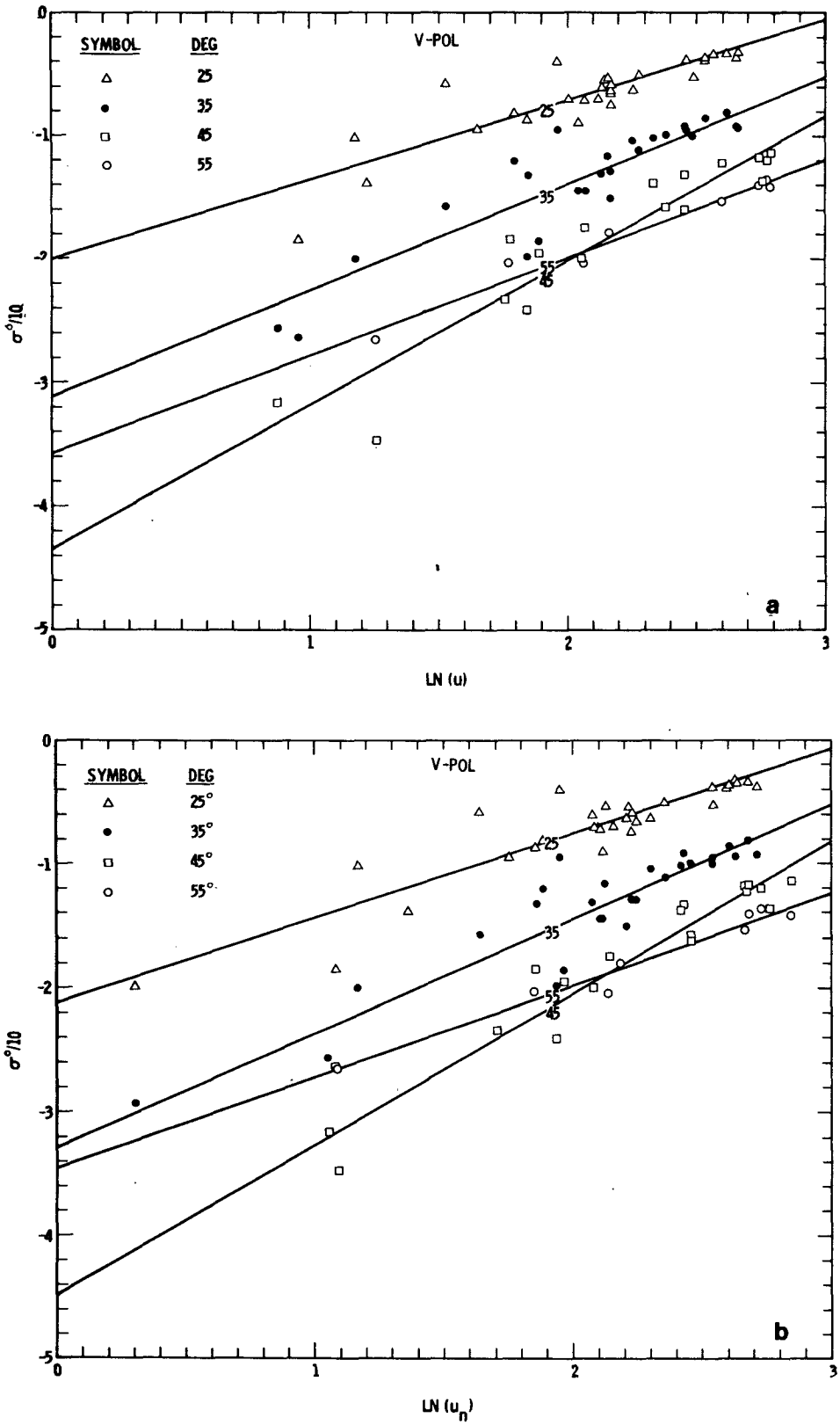

FIG. 6. Data points and regression lines for adjusted σ° versus (a) u and (b) u_N, for $\theta = 25, 35, 45$ and $55°$. Vertical polarization.

TABLE 2. Comparison of observed σ° with derived σ° given incidence angle and azimuth angles of Seasat and wind speed and direction from surface truth. Columns indicate polarization, incidence angle, correlation coefficient, slope of regression line, y intercept, mean absolute difference between the observed and derived σ°, mean difference, standard deviation of the absolute difference, standard deviation of the difference and sample size.

Polarization	θ_i	r	m	b	$\overline{\lvert\sigma^\circ_{TH} - \sigma^\circ_0\rvert}$	$\overline{(\sigma^\circ_{TH} - \sigma^\circ_0)}$	σ_A	σ_D	Size
H	25	0.873	1.014	−2.55	3.13	−2.69	2.70	3.14	121
H	35	0.869	0.982	−3.19	3.46	−2.89	2.91	3.48	69
H	45	0.945	1.170	2.31	2.20	−1.59	1.82	2.36	45
H	55	0.809	1.048	0.248	2.79	−1.00	3.28	4.19	25
V	25	0.880	1.072	−1.50	2.57	−2.22	2.52	2.83	130
V	35	0.916	0.941	−3.20	2.62	−2.29	1.90	2.29	64
V	45	0.926	0.900	−2.79	1.86	−0.886	1.41	2.16	67
V	55	0.936	1.381	4.65	3.31	−3.13	3.28	3.45	27

and so on for 35, 45 and 55°. Statistics generated in this study are found in Table 2.

Again, V polarization seems to be better than H polarization in almost every category but there are exceptions, especially at 55°. It is important to note the large scatter demonstrated by the standard deviations of the differences and absolute differences, σ_D and σ_A. Scatter of the order of 3 dB, as found here, can translate into errors ~3–4 m s^{-1}. These cannot be improved by simply adjusting for stability and height. It is also interesting to note that although the mean difference is always negative, the y intercept changes sign for high incidence angles, indicating an incidence-related bias. The differences between the absolute and actual errors (i.e., the columns showing the average absolute and actual differences) indicate that there is about a 0.5 dB offset that is due to scatter about the mean, with the rest of the error being due to actual bias in the data. The differences indicate that the model-produced σ°'s are always lower then the observed when surface truth winds and angles are used. This is the same as saying that the algorithm would yield winds which are above the observed values if SASS σ°'s were used. This is in keeping with the findings of Jones *et al.* (1979) in their analysis of GOASEX data. The findings here, however, indicate that this bias is incidence-angle-dependent. Fig. 7 shows the regression line and related points at $\theta = 45°$ for V polarization. Note how the scatter tends to increase at low σ° values which correspond mostly to low winds. Most of the data seem to cluster in a comparatively limited range demonstrating the need for a greater variety of conditions for verification, especially those with strong winds.

6. Summary and conclusions

Both theoretical and experimental results have been presented which compare the behavior of winds in the surface layer with SASS data. The theoretical investigation focused on what errors can be expected by ignoring stability or height factors when comparing σ° to winds or wind stress. Results show that deriving neutral winds at a standard height will mitigate errors. Using u^* as the standard parameter makes choosing a "correct" u^*–z_0 fundamental. Stability effects can generally be ignored in unstable atmospheres but not in stable atmospheres. Height adjustments are significant only if some of the observations lie close to the surface (<5 m) where the logarithmic profile becomes pronounced.

In comparing SASS σ° values with GOASEX surface truth, these considerations seem of secondary importance. σ° does seem to correlate well with the log of the wind speed, but no improvement can be detected in comparing with wind stress or neutral wind. This is probably due to the large scatter present in the available SASS data with standard deviations near 3 dB in some cases. Vertical polarization performs better, in general, than horizontal. Incidence angles > 50° also behave anomalously, but this may be a factor of the sample size.

Some of the reasons for the large scatter are due to the instruments and some due to the ocean and weather conditions. Both the SASS and the ship or buoy anemometers produce errors which must be taken into account. Anemometers were used in the original calibration of scatterometers which produced the algorithms in use today. The sampling error as reported by Pierson *et al.* (1979) also enters the comparison and can contribute up to ±1 m s^{-1}. The SASS instrument errors are as yet unknown in themselves. Some underflights during the Seasat mission were able to provide calibration data for SASS. It was determined (L. Jones, personal communication) that biases were present in the four beams, but they were not equal. The biases, however, were only on the order of a few tenths of a decibel.

The major portion of the scatter is probably due to problems in obtaining accurate parameters for (1) and in verifying them against available surface truth. Variations in atmospheric conditions, especially in the presence of thick clouds and precipitation, could

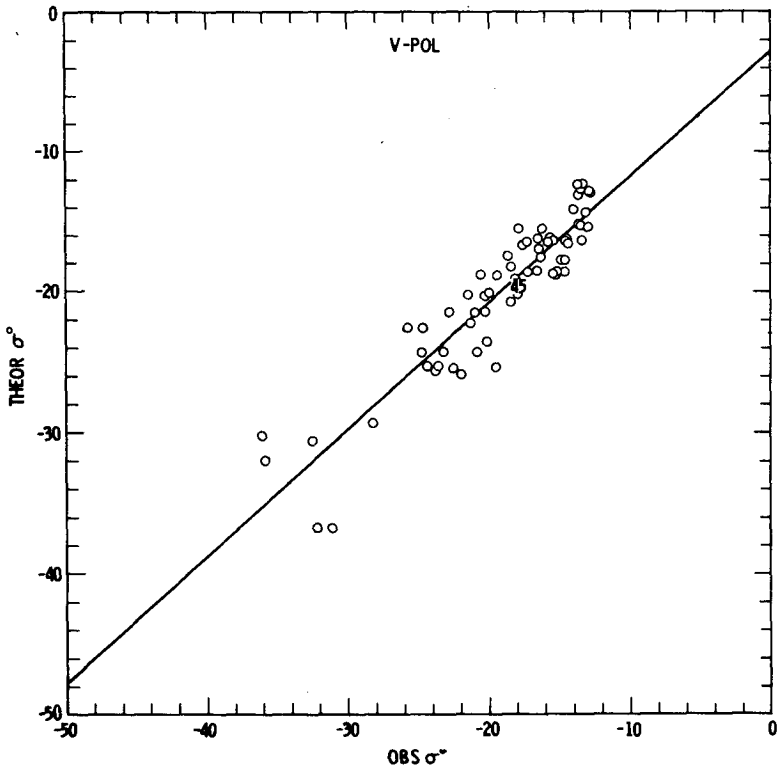

FIG. 7. Theoretical σ° versus observed SASS σ° for $40^\circ < \theta \leq 50^\circ$. Vertical polarization.

create attenuated readings which show up as poor statistics. In the current analysis, these factors were not filtered from the data, so that rain areas were counted along with clear areas in the comparison. Adverse ocean conditions in the form of man-made or natural slicks were also included with the other data. Spatial interpolation can also add to the error. Despite the proximity and density of the σ° data, points lying some 70 km from the observation point may have encountered wind speeds and directions significantly different from those at the anemometer. The interpolation scheme would then blend the entire inhomogeneous field into one σ° resulting in appreciable interpolation error. Turning of the wind in the surface layer may also be a source of error. It is assumed that the turning angle of the wind in the surface layer is generally $< 10^\circ$. But in shallow surface layers, differences between wind directions at 10 or 20 m and the surface could account for serious σ° scatter.

At present it is almost impossible to ascertain the chief source of error for SASS, but investigations are under way to analyze both the surface truth and SASS output to determine what may be the chief cause of scatter. Until the causes of scatter can be controlled, corrections for surface layer effects will be inconsequential. Comparisons with u, u_N or u^* will look essentially the same, as demonstrated here. In the future, a closer look at more surface truth and its related σ° fields will be made in order to increase the sampling size for all incidence angles.

Acknowledgments. Thanks are due to W. J. Pierson and R. Salfi for their assistance in securing surface truth. The author is also grateful to the entire SASS experiment team for their cooperation in providing σ° data for comparison. Special thanks are due to Dr. D. Boggs for securing the proper data tapes and programs for the performance of some of these experiments.

This research was carried out at the Jet Propulsion Laboratory, California Institute of Technology, under NASA Contract NAS 7-100.

APPENDIX

Iterative Procedures for Deriving u^* in the Unstable Atmosphere

Using Eqs. (3) and (4), one may obtain the following implicit relationship for L:

$$L = \bar{\theta}_v u^{*2}[\ln z/z_0 + \psi_h(z/L)](gk^2\Delta\theta_v)^{-1}. \quad \text{(A1)}$$

The stress parameter u^* must also fit the relationship derived from (3), i.e.,

$$u^* = ku[\ln z/z_0 + \psi_h(z/L)]^{-1}. \quad \text{(A2)}$$

If z_0 were constant, the expression for u^* found in (A2) could be inserted in (A1) and a single implicit relationship found for L. However, since z_0 is assumed to vary with u^*, it is necessary to iterate about u^* until convergence is reached. To insure convergence within this complicated framework, the bisection method can be used on u^*. This involves choosing limits on u^* and selecting the midpoint as a guess. If the guess proves too high (low), it becomes the new upper (lower) bound and the new midpoint selected as a guess. As a lower limit, the neutral value of u^* is selected [i.e., the solution of $ku = u^* \times \ln z/z_0(u^*)$, which can easily be derived for each of C, P and G]. A practical upper bound to u^* could be ku, since generally $z \gg z_0$. When the guess u_n^* is made, L is found by using a Newton-Raphson iteration which gives

$$L_{m+1} = L_m - (L_m - \bar{\theta}_v u^{*2}\{[\ln z/z_0 + \psi_h(z/L_m)](gk^2\Delta\theta_v)^{-1}\}) \times [1 - \bar{\theta}_v u^{*2}\psi_h'(z/L_m)(gk^2\Delta\theta_v)^{-1}]^{-1}, \quad \text{(A3)}$$

where the subscript refers to the guess and ψ_h' is the derivative of ψ_h with respect to L. Once $|L_{m+1} - L_m| < \epsilon$ for some specified convergence criterion, L is set to L_{m+1} and used in (A2), along with u_n^* and $z_0(u_n^*)$. If u_n^* is larger (smaller) than the right-hand side of (A2), then u_n^* is made the new upper (lower) bound and u_{n+1}^* is found. Convergence is retarded somewhat because z_0, on the whole, tends to increase as u^* does. Thus, raising u^* also raises the rhs of (A2), the effect of $\psi_h(z/L)$ being negligible for the most part. But since z_0 is contained in a logarithmic expression, its influence is limited and convergence is eventually reached. One must be careful also to allow only negative values of L in the iteration. (A3), which in effect sets an upper bound on L of approximately $-9z/4$. Otherwise, $|\psi_h(z/L)| > \ln z/z_0$ and L becomes positive for negative $\Delta\theta_v$, a distinctly physical impossibility. Values of L larger than $-9z/4$ are akin to free convection and the surface layer must be dealt with in accordance with free convective rather than mechanical convective theory.

REFERENCES

Born, G. H., J. A. Dunne and D. B. Lame, 1979a: Seasat mission overview. *Science*, **204**, 1405–1406.

——, D. B. Lame and J. C. Wilkerson, 1979b: GOASEX Workshop Report. Rep. 622-101, Jet Propulsion Laboratory, Pasadena, CA.

Bradley, G. A., 1971: Remote sensing of ocean winds using a radar scatterometer. Ph.D. thesis, University of Kansas, 213 pp.

Businger, J. A., J. C. Wyngaard, Y. Izumi and E. F. Bradley, 1971: Flux-profile relationships in the atmospheric surface layer. *J. Atmos. Sci.*, **28**, 181–189.

Cardone, V. J., 1969: Specifications of the wind distribution in the marine boundary layer for wave forecasting. New York University Rep. TR69-1, 67 pp.

——, J. P. Young, W. J. Pierson, R. K. Moore, J. A. Greenwood, C. Greenwood, A. K. Fung, R. Salfi, H. L. Chen, M. Afarami and M. Komen, 1976: The measurement of the winds near the ocean surface with a radiometer scatterometer on Skylab. NASA-JSC Contract NAS 9-13642, Final report E-PN550, prepared jointly by City University of New York and the University of Kansas CRES, Houston, TX.

Charnock, H., 1955: Wind stress on a water surface. *Quart. J. Roy. Meteor. Soc.*, **81**, 639–640.

Dyer, A. J., 1967: The turbulent transport of heat and water vapor in an unstable atmosphere. *Quart. J. Roy. Meteor. Soc.*, **93**, 501–508.

Garratt, J. R., 1977: Review of drag coefficients over oceans and continents. *Mon. Wea. Rev.*, **195**, 915–929.

Gonzalez, F. I., and SAR Team, 1979: Seasat Synthetic aperture radar: Ocean wave detection capabilities. *Science*, **204**, 1415–1421.

Hühnerfuss, H., W. Alpers and W. Linwood Jones, 1978: Measurements at 13.9 GHz of the radar backscattering cross section of the North Sea covered with an artificial surface film. *Radio Sci.*, **13**, 979–983.

Jones, W. L., and L. C. Schroeder, 1978: Radar backscatter from the ocean: Dependence on surface friction velocity. *Bound.-Layer Meteor.*, **13**, 133–149.

——, —— and J. L. Mitchell, 1978a: Aircraft measurements of the anistropic microwave scattering signature over the ocean for the 1975 JONSWAP and 1976 East Coast Mission. NASA TM 28646, NASA Langley Research Center, 22 pp.

——, F. J. Wentz and L. C. Schroeder, 1978b: Algorithm for inferring wind stress from Seasat-A. *J. Spacecraft Rockets*, **15**, 368–374.

——, and the SASS Team, 1979: Seasat Scatterometer: Results of the Gulf of Alaska Workshop. *Science*, **204**, 1413–1415.

Kitaigorodskii, S. A., and M. M. Zaslavskii, 1974: A dynamical analysis of the drag conditions at the sea surface. *Bound.-Layer Meteor.*, **6**, 53–61.

Lipes, R. G., and the SMMR Team, 1979: Seasat scanning multichannel microwave radiometer: Results of the Gulf of Alaska Workshop. *Science*, **204**, 1415–1417.

Lo, A. K., 1977: An analytical-empirical method for determining the roughness length and zero-plane displacement. *Bound.-Layer Meteor.*, **12**, 141–151.

Moore, R. K., and W. J. Pierson, 1971: Worldwide oceanic wind and wave predictions using a satellite radar-radiometer. *J. Hydronaut.*, **5**, 52–60.

——, A. K. Fung, G. J. Dome and I. J. Birrer, 1979: A technique to estimate the wind vector over the ocean from orthogonal radar scatterometer measurements—Windvec algorithm. RLS TR 343-2, University of Kansas, 34 pp.

Phillips, O. M., 1977: *The Dynamics of the Upper Ocean*. Cambridge University Press, 334 pp.

Pierson, W. J., 1978: Verification procedures for the Seasat measurements of the vector wind with the SASS. Report to JPL Contract 954411, City University of New York, 34 pp.

——, and R. Salfi, 1978: The theory and data base for the CUNY SASS wind algorithm. Final Report to JPL, Contract 954411, City University of New York, 103 pp.

——, and Stacy, R. A., 1973: The elevation slope and curvature spectra of a wind-roughened sea surface. NASA CR-2247, Washington, DC, 28 pp.

——, R. Salfi, R. S. Dischel and G. Baeslack, 1979: Measuring winds with anemometers and the Seasat scatterometer. NASA Langley Research Center, Contract NAS-15669, Technical report by City University of New York, 105 pp.

Ross, D., and W. L. Jones, 1978: On the relationship of radar backscatter to wind speed and fetch. *Bound.-Layer Meteor.*, **13**, 151–163.

Tapley, B. D., and the Altimeter, 1979: Seasat altimeter calibration: Initial results. *Science*, **204**, 1410–1412.

Young, J. D., and R. K. Moore, 1977: Active microwave measurement from space of sea-surface winds. *IEEE J. Ocean. Eng.*, **2**, 309–317.